Chapter 1

Introduction

1.1 Why study the Io footprint?

Solar system planets are usually seen as huge balls of rock or gas limited to their planetary radius. However, their influence on the surrounding environment extends much beyond the upper limit of their atmosphere.

Their gravitational influence enables a variety of smaller astronomical objects to orbit around them. Jupiter, for instance, is surrounded by a multitude of satellites (63 have been observed so far). Four particularly big moons, Io, Europa, Ganymede and Callisto stand among these satellites. These moons are called Galilean satellites, after their discovery by Galileo Galilei in 1610. The present study focuses on Io, which is both the closest and the most turbulent of these four. Its surface is spotted with erupting volcanoes that project plumes of material up to 300 km in altitude.

Planets also have an electromagnetic sphere of influence, a region where phenomena are dominated or organized by the planetary magnetic field. These regions may be pictured as cavities dug into the solar wind and are called magnetospheres. Aurorae are radiative emissions resulting from the precipitation of high energy particles into the planetary atmosphere. They are often considered as the imprint of the different phenomena occurring inside the magnetosphere. This view is particularly relevant for the subject of this work: the Io footprint. The goal of this study is to understand the auroral feedback which arises when the most volcanic body of the solar system meets the most strongly-magnetized planet.

The Io ultraviolet (UV) auroral footprint is one of the most spectacular consequences of the strong interaction between Io and the magnetosphere of Jupiter. It consists of bright spots visible in both hemispheres of Jupiter's atmosphere. Their

latitude is a few degrees equatorward from the main polar aurorae and their longitude is linked to the orbital position of Io with respect to Jupiter. Recent studies showed that these spots can be multiple and are followed by a faint trailing tail of UV emissions (*Clarke et al.*, 2002; *Gérard et al.*, 2006). These studies also demonstrated that the brightness of the Io spots is evolving with typical timescales of hours. The objective of the present work is to characterize as precisely as possible the morphology and the dynamics of these footprint spots in order to unveil the mechanisms that cause them.

The observable signature of the Io-Jupiter interaction is not a unique exotic phenomenon. The finding of similar interactions with Europa and Ganymede has led to the conclusion that the Io case could be the paradigm of a possibly widespread phenomenon in the universe. It is most likely that similar interactions could occur between an exoplanet and its satellites, and the same kind of mechanism has also been proposed for the interaction between a planet orbiting a white dwarf or between a magnetic and a non-magnetic white dwarf (*Bhardwaj and Michael* (2002)). However, the most dramatic examples of similar interactions have been recently found to take place between an exoplanet an its parent star. In the last decade, several cases of periodic enhancements of the chromospheric emissions of stars correlated with the orbital period of giant planets in a close orbit have been found (*Shkolnik et al.*, 2003; *Shkolnik et al.*, 2005). Additionally, photometric satellite observations performed by MOST (*Walker et al.*, 2008) and CoRoT (*Pagano et al.*, 2009) also found evidences for stellar spots caused by a magnetic interaction between exoplanets and their parent stars.

The first clues for the Io-Jupiter interaction come from the radio domain and the first evidence for light emissions on Jupiter related to Io were found in the infrared (IR) wavelengths. However, thanks to the successive improvements of the Hubble Space Telescope (HST) instruments, the richest database concerning the Io footprint currently lies in the far ultraviolet (FUV) domain. Several early studies have been carried out based on HST data, which unraveled some essential characteristics of the Io footprint. However, many grey areas still remained concerning the ongoing mechanisms related to the Io-Jupiter interaction and some early results appear to be contradictory.

1.2 Outline of the thesis

This thesis is divided into two parts, spreading over nine chapters. A large part of my contribution to the study of the Io footprint consisted of resolving technical image processing issues that were not specifically related to the footprint. Among these tasks were the construction of a standardized database containing all the existing high-resolution FUV observations of the Jovian aurorae and the compilation of a complete catalog of all these images and spectra. Another task was the development of automatic methods to find the planetary center and orientation on the images. Therefore, I have deliberately isolated most of the technical discussions related to the dataset and images processing in Chapter 2. The idea is to separate the common technical issues from the detailed analysis and interpretation of the different Io footprint characteristics. Moreover, these methods have also been developed so that they can be applied to other studies using HST images, both for Jupiter and Saturn. Some readers might be only interested in this technical part and not in Io footprint related issues. In addition to these generic image processing procedures, I have been given the opportunity to apply a method that I specifically developed for characterizing the Io footprint tail (see Chapter 5) to the main auroral emissions at Saturn. Consequently, I decided to report the outcome of this latter study in Appendix 1.

The second part of my thesis, which actually constitutes the core of the present work, is formed by this introduction and chapters 3 through 8. The goal of this part of my thesis is to demonstrate that a careful analysis of the Io footprint characteristics on the HST FUV images from the STIS and ACS instruments can provide us with crucial information to understand the Io-Jupiter electromagnetic interaction. The present manuscript is articulated around five basic questions:

- What is the Io footprint? (Chapter 3)
- Where is the Io footprint? (Chapter 4)
- How high is the Io footprint? (Chapter 5)
- How big is the Io footprint? (Chapter 6)
- How bright is the Io footprint? (Chapter 7)

We will see that the answer to each of these questions has very profound implications for the Io-Jupiter electromagnetic interaction and its underlying physics. However,

my approach is not inductivistic. Various theoretical models have made predictions for these different quantities. In each case, these predictions were tested against the observations. As a result, some models were validated while others were discarded. However, the most interesting cases arise when the observational results do not match any previous model expectations. It is then necessary to propose alternative interpretations and test them against other types of measurements.

Before diving into the detailed exploration of the Io UV footprint, I will present briefly the two actors of the celestial play we are concerned with: Jupiter and its magnetosphere on one side and Io on the other. A section is also dedicated to the different models that have been developed in order to describe the interaction. Then, the observations related to Io-Jupiter interaction are examined. These observations are the starting point of our investigations. Finally, the last section of the introductory chapter consists of a short description of the two instruments that have been considered in the present work.

1.3 Coordinate systems

Since Jupiter is a gaseous planet, no coordinate system can be related to the crustal rotation as is the case for rocky or icy bodies. Consequently, several coordinate systems have been defined relative to the motion of the cloud bands or to the rotation of the magnetic field.

As far as the polar aurorae are concerned, the most relevant coordinate system is the so-called System III, since the main auroral features are approximately fixed in this reference frame. This coordinate system is bound to the Jovian magnetic field. More precisely, it is defined by the rotational period of decametric radio sources in Jupiter's ionosphere. This coordinate system is left-handed, i.e. the longitudes increase from dusk to dawn through noon. The System III longitude of the intersection point of the Earth-Jupiter line with the Jovian surface (i.e. the sub-Earth longitude) is called the Central Meridian Longitude (CML).

Another coordinate system is widely used, notably for describing the position of the moons relative to the observer on the Earth. The reference meridian is fixed relative to the Earth-Jupiter line, 0° being in the anti-Earth direction. This coordinate system is right-handed, i.e. the longitudes increase from dawn to dusk through noon.

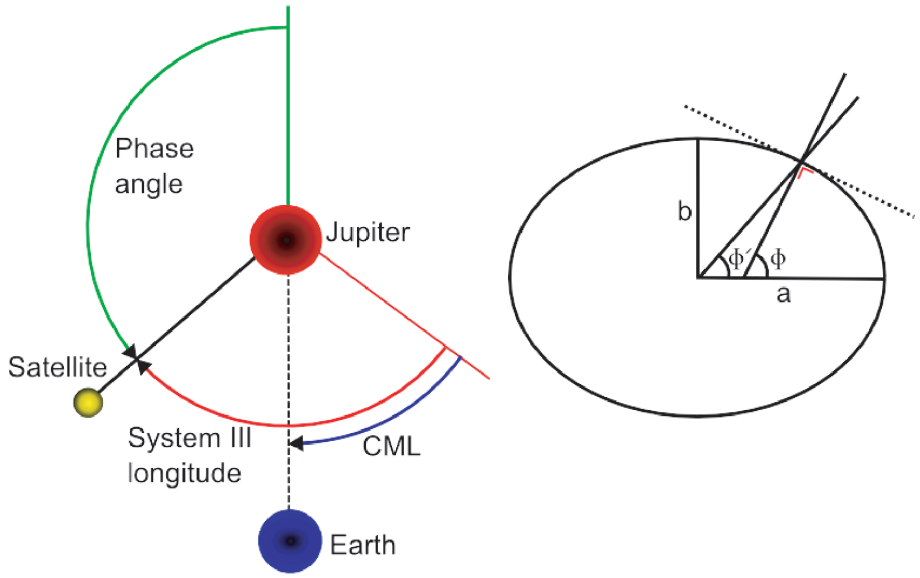

Figure 1.1: (Left) Illustration of the System III coordinate system and the phase angle. The green arc represents the phase angle of the satellite. The red arc represents its System III longitude. The blue arc represents the central meridian longitude (CML). (Right) Illustration of the planetocentric (Φ') and planetographic (Φ) latitudes.

Since Jupiter's shape is an ellipsoid[1], two latitude systems also co-exist: the planetocentric (or jovicentric in this case) and the planetographic (or jovigraphic) latitudes. The first one (Φ') refers to the angle between the line joining the planet center to the considered point and the equatorial plane, while the second one (Φ) refers to the angle between the normal to the surface at the considered point and the equatorial plane. These two angles are related by the following formula:

$\tan(\Phi') = \frac{b^2}{a^2}\tan(\Phi)$

where a is the semi-major axis of the ellipsoid and b the semi-minor axis.

1.4 The Jovian magnetosphere

Eight spacecrafts have carried out in-situ observations of Jupiter's magnetosphere, most of them during single fly-bys of the giant planet. The first were Pioneer 10 and Pioneer 11, respectively in 1973 and 1974. Then followed Voyager 1 and Voyager 2 in 1979 and 1982 respectively, and the solar wind explorer Ulysses in 1992. The latter

[1]The equatorial radius is 71492 ± 4 km and the polar radius is 66854 ± 10 km (*Weiss*, 2004).

is the only one which did not probe the Jovian magnetosphere within the equatorial plane but crossed it from North to South. The Galileo spacecraft is the first and the only Jovian orbiter so far. Its orbit insertion occurred in 1995 and it operated for eight years before being navigated into Jupiter's atmosphere at the end of the mission lifetime. During the Galileo era, the Cassini spacecraft encountered Jupiter in late 2000 before reaching Saturn, its final destination, in 2004. The spacecraft which flew by Jupiter most recently was New Horizons in February 2007, on its way to Pluto and beyond. This last opportunity of in-situ measurements inspired the Hubble Space Telescope large observation campaign discussed below (see Chapter 2) and which constitutes the core of our image database.

The Jovian magnetosphere is the largest magnetosphere of the solar system. The distance from the planet center to the dayside magnetopause can reach ∼100 Jovian radii (R_J), while the limit is only ∼10 Earth radii for our planet. If Jupiter's magnetosphere were visible to the naked eye, it would appear bigger than our moon in the sky. Jupiter's internal magnetic dipole axis is tilted by 9.6° from the rotation axis of the planet and its rotation period is 9h55m. As stated in Section 1.3, the System III longitudes as well as the global shape of the aurorae are fixed relative to the magnetic field. The Jovian magnetosphere differs from the Earth's in two main aspects: the plasma source and the energy source. The Earth magnetosphere is a solar wind-driven magnetosphere in which both the plasma and the energy mainly originate from the solar wind. Jupiter's magnetosphere is an internally-driven magnetosphere and the available energy is mainly provided by the rapid rotation of the planet's strong magnetic field. Additionally, the magnetospheric plasma essentially originates from an internal source: Io's volcanism. Io and its surrounding environment provide approximately 1 ton/s of plasma into the Jovian magnetosphere[2] while the solar wind and the atmospheric escape from Jupiter only provide <100 kg/s and ∼ 20 kg/s respectively (*Khurana et al.*, 2004).

The Jovian magnetosphere is usually divided into 3 regions: the inner magnetosphere, the middle magnetosphere and the outer magnetosphere. The inner magnetosphere is mainly controlled by the Jovian internal magnetic field. The main features are the inner radiation belts and the Io plasma torus which stands from 5 to 10 R_J. The latter is a doughnut shaped reservoir of charged particles origi-

[2]This value of 1 ton/s is in fact the quantity of neutrals provided by Io, however about half of them experience charge exchange processes and escape from the Jovian system as energetic neutral atoms (ENAs) (*Dols et al.*, 2008).

nating from Io's intense volcanism (see next section). In the inner magnetosphere, the rapidly rotating internal magnetic field enforces the plasma to corotate with the planet. Two processes drive auroral emissions in this region: the Io-magnetosphere interaction and the plasma injections. The first mechanism is the core of the present work and will be described in detail in the next sections. The second feature involves injections of hot plasma which suddenly move inwards and then drift with respect to the bulk rotational flow of plasma in an energy-dispersed way (i.e. low energy electrons drift faster than the high energy ones). Their auroral signatures are System III-fixed patchy emissions as seen on Figure 1.2.

The middle magnetosphere spans from 10 to 40 R_J. In this region, the internal field influence weakens and the azimuthal currents radially distort the field lines and confine the plasma into a thin current sheet (see Figure 1.3). Additionally to their azimuthal motion, the field lines loaded by the iogenic plasma slowly migrate outward while emptied flux tubes move inward. When the ionosphere-magnetosphere interaction becomes insufficient to provide enough angular momentum to the plasma, the initially rigid corotation of the equatorial plasma disk progressively breaks down with increasing distance. This process involves radial currents which close through field aligned currents and ionospheric Pedersen current, forming a current loop. It is the large field aligned potentials generated by the equatorward branch of the current loop which are thought to be responsible for the main aurora (see review in *Clarke et al.*, 2004).

The outer magnetosphere ranges from 40 R_J to the magnetopause. It is the region where the internally driven Vasyliunas reconnection cycle takes place (*Vasyliunas*, 1983). On Earth, tail reconnections are triggered by the solar wind activity, forming the so-called Dungey cycle. On Jupiter, the tail reconnections observed every 2-3 days are caused by the continuous mass loading of the magnetotail field lines. At some point, the magnetic tension is no longer able to compensate for the centrifugal force, so that reconnections occur and plasmoids are released with a typical period of 2 to 3 days (Figure 1.4). The faint and transient spots observed directly poleward from the main auroral oval are related to this phenomenon (*Grodent et al.*, 2004; *Radioti et al.*, 2008b). The highly variable polar auroral emissions are also related to the processes taking place in the outer magnetosphere. Some authors have suggested that some of these emissions could be related to an Earth-like solar wind driven Dungey reconnection cycle (*Cowley et al.*, 2003; *Grodent et al.*, 2003b). However, *McComas and Bagenal* (2007) argued that the rotational and

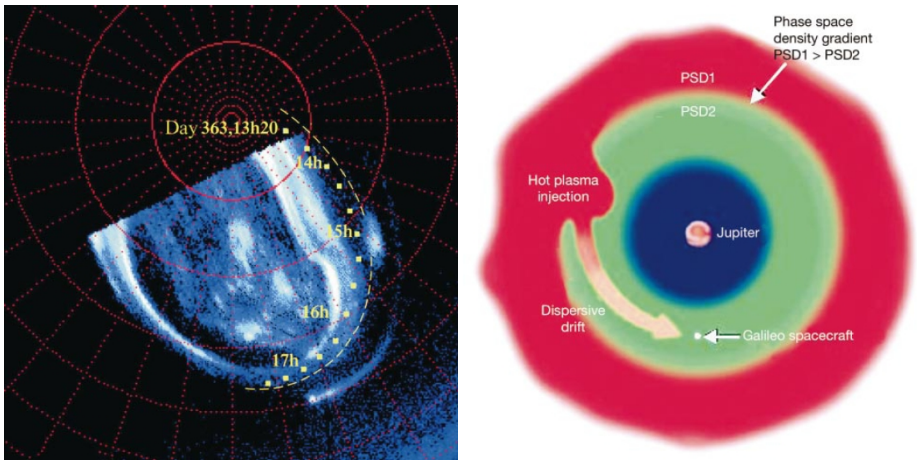

Figure 1.2: (left) Polar projection of the northern aurora simultaneous to Galileo plasma injection observations. The luminous patch related to these injections is the large spot close to the "15h" indication. (right) Illustration of the process explaining both Galileo and HST observations. Hot plasma is rapidly injected into the inner magnetosphere and then experiences a dispersive drift (from *Mauk et al.*, 2002).

convection timescales on Jupiter and on Earth are so different that Jovian reconnections should preferentially take place on the magnetopause flanks instead of in the central magnetotail.

The location of the Jovian magnetopause strongly depends on the solar wind dynamic pressure, so that the dayside magnetopause distance typically fluctuates from ∼45 to 100 R_J. On the nightside, the magnetotail extends as far as the orbit of Saturn.

1.5 The Io-Jupiter interaction

1.5.1 Orbits and tides

In the remainder of this work, I will assimilate the Io-Jupiter interaction to the electromagnetic interaction. However, this is not the only interaction coupling Jupiter's and Io's fates. The gravitational interaction is the root cause for Io's volcanism through tidal heating. An important feature of Io, Europa and Ganymede is that their orbit periods are integer multiples of each other. Io rotates twice as fast as Europa, which in turn rotates twice as fast as Ganymede. This resonance (called a Laplace resonance) enhances the orbits' eccentricities, since the moons are sys-

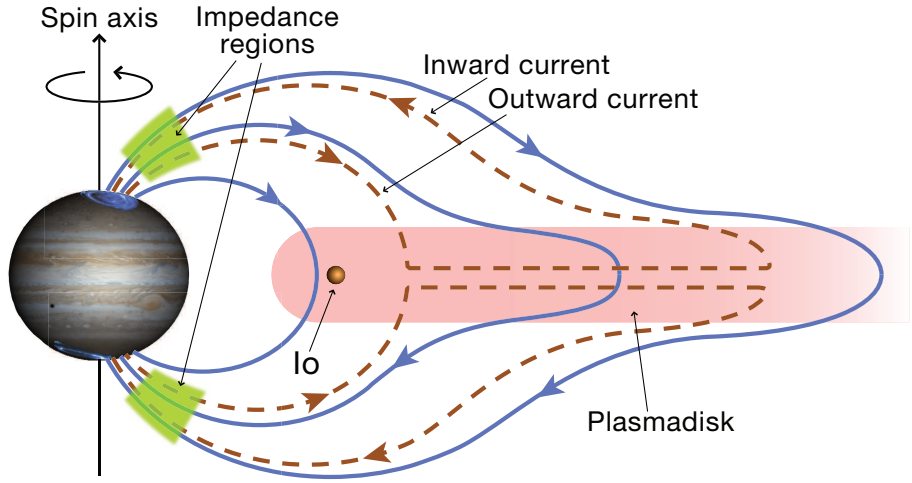

Figure 1.3: Illustration of the inner and middle magnetosphere. Io, located at 6 R_J is the main source of the magnetospheric plasma. The ionized particles are first located in a dense plasma torus along the Io orbit and corotate with the magnetic field. This plasma is also slowly migrating outward, feeding the rest of the magnetosphere. This diffusing plasma is essentially confined in the current sheet. The azimuthal current in the current sheet distends radially the magnetic field lines (blue solid lines). The current loop formed by the radial component of the current sheet, the field aligned currents and the Pedersen current in the ionosphere transfer angular momentum from the ionosphere to the plasma and is represented by the red dashed line (from *http://lasp.colorado.edu/~bagenal/JPO/diagrams.html*).

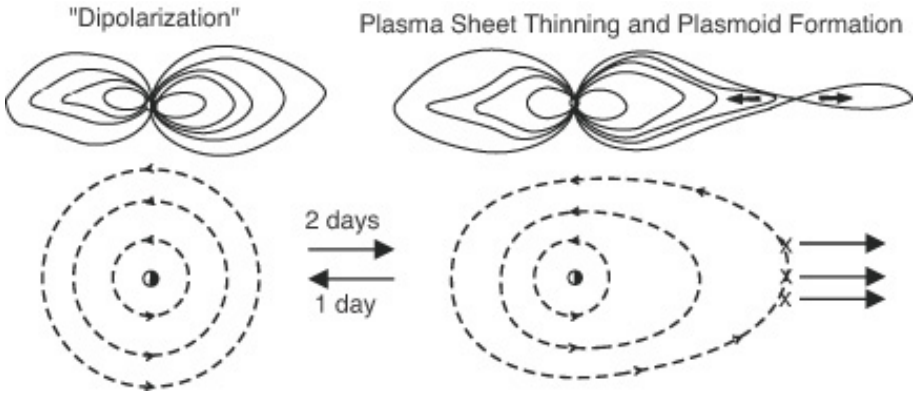

Figure 1.4: Illustration of the internally driven reconnection cycle. Starting from a relatively dipolar configuration, the newly injected plasma from Io progressively loads the flux tubes, leading to the thinning of the plasma sheet. When the magnetic tension becomes unable to counterbalance the centrifugal forces, reconnections occur, plasmoids are released and the magnetosphere comes back to the initial dipolar configuration (from *Krupp et al.*, 2004).

tematically pulled in the same direction at the same location on their orbit. The proximity of the giant planet creates a bulge on Io and forces Io's spin period to be equal to its orbit period. If Io's orbit were perfectly circular, the bulge would always face Jupiter. However, Io's orbit is an ellipse and the moon is orbiting faster than it is spinning at perijove, while it is spinning faster than it is orbiting at the apojove. Additionally, since the gravitational forces are stronger at the perijove, the bulge is also larger. All these processes conspire to mix Io's lower mantle material, and this tidal heating provides a considerable amount of energy (on the order of 5×10^{13} W).

The gravitational interaction not only has an impact on Io's tides, but it also triggers tides on Jupiter. Both Io's and Jupiter's tides affect Io's orbital dynamics. Jupiter's fast spinning pulls the bulge created by Io towards the leading direction (see Figure 1.5). The consequences are a deceleration of Jupiter's rotation and an increase of Io's orbital velocity, which sends Io further away from Jupiter. Focusing now on Io at the perijove, Io's bulge is lagging compared to the orbital motion, which tends to accelerate Io's rotation but slows down Io along its orbit. The effects of Io's bulge are opposite at the apojove, but since Io is further out, the consequences are not as important. Thus, in total, Io's tidal effect tends to bring it closer to Jupiter.

We can notice that Jupiter's tides tend to move Io inwards while the Io tides tend to move Io in the opposite direction. A recent study (*Lainey et al.* (2009)) demonstrated that since 1891, Io has moved 55 km inward while Europa and Ganymede

have moved outward by 125 km and 365 km, respectively. Consequently, the authors concluded that the three moons' orbital periods are slowly evolving away from the Laplace resonance. The long term consequence will be that Io's orbit will become more circular and that the strong volcanism will most probably vanish. The following sections reveal that this prediction will have important consequences for the Jovian auroral activity.

1.5.2 Io and the plasma torus

Even though the situation could plausibly change in the long term, Io is currently the most volcanic body of the solar system. More than 100 active volcanoes have been detected on its surface. This volcanism is the source of Io's tenuous atmosphere, mainly made of SO_2. This atmosphere loses mass to the Jovian magnetosphere and beyond at a rate on the order of 1 ton per second. Consequently, Io is the main source of the Jovian magnetospheric plasma. This Iogenic plasma is mostly made of ions originating from the SO_2 molecule, i.e.mainly S^+, S^{++}, S^{+++}, O^+ and O^{++}. A fraction of this plasma is directly picked-up from Io's exosphere. Another population of the atmospheric particles escapes from Io's gravitational influence as neutrals and forms an extended (more than $\sim$10 R_{Io}) neutral cloud around the satellite. These neutrals can then be ionized through electron impact and charge exchange. This neutral cloud is expected to be the main mass and energy source for the plasma torus (*Dols et al.*, 2008). Presumably, newly created plasma first remains at rest in the wake of Io. These particles are then accelerated up to corotation with the Jovian magnetic field through electromagnetic coupling with Jupiter (see Section 1.5.4.6). The strong magnetic field of Jupiter confines this dense plasma along Io's orbit and forms the plasma torus. Io rotates around Jupiter at 17 km/s while the plasma torus rotates at 74 km/s. The plasma stream velocity relative to Io is thus 57 km/s. The plasma torus is latitudinally confined around its centrifugal equator, which is different from both the rotational and magnetic equators of Jupiter. This equatorial plane is tilted relatively to the Io orbital plane because of the tilt of the Jovian magnetic field (see Figure 1.6a). As a consequence, Io's centrifugal latitude evolves with the Jovian rotation, moving from the northern border of the torus to its southern border and *vice-versa*, as a function of the System III longitude of Io (see Figure 1.6b). In addition to the tilt of the centrifugal plane, the torus is shifted to the dawn side because of the East-West electric field in the Jovian magnetosphere

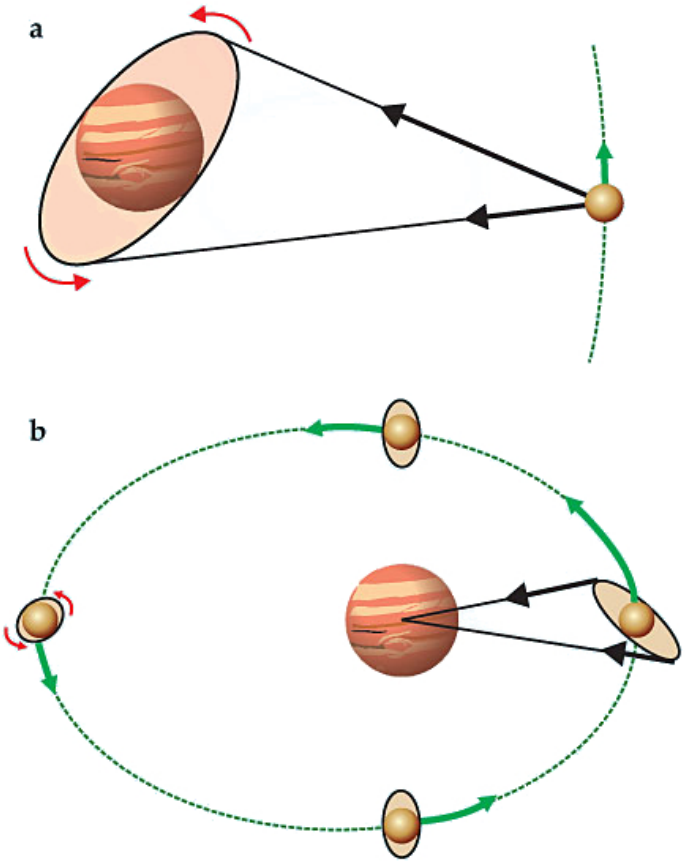

Figure 1.5: Tides in Jupiter and its innermost large moon, Io, have opposite effects on Io's orbit. (a) Io's gravity creates a tidal bulge in Jupiter, which is pushed by Jupiter's rotation (red arrows) ahead of the Io–Jupiter line. Gravitational interaction (black arrows) between Io and the bulge slows Jupiter's rotation and increases Io's orbital energy. (b) Jupiter also creates a tidal bulge in Io. Because Io has an elliptical orbit, its instantaneous orbital speed varies (green arrows). At its most distant point from Jupiter, Io rotates (red arrows) faster than it orbits, so the bulge lies slightly ahead of the Io–Jupiter line in the direction of Io's rotation. At its nearest point to Jupiter, the opposite is true. As a result, Jupiter exerts a force on Io that diminishes Io's orbital energy. The tidal bulges and orbit eccentricity are exaggerated for clarity. (adapted from *Miller* (2009))

(*Smyth and Marconi*, 1998).

1.5.3 The local electromagnetic interaction

In their review of the magnetic interactions of satellites with the giant planets' magnetospheres, *Jia et al.* (2009a) distinguish four categories of satellites:

- inert satellites (such as Tethys, Rhea),
- satellites with an intrinsic magnetic field (Ganymede),
- satellites with an internally induced magnetic field (Europa, Callisto) and
- satellites with significant neutral sources and strong plasma interactions (Io, Enceladus, Titan).

Galileo observations demonstrated that Io has no significant internal magnetic field, whether induced or intrinsic. However, Io has a neutral atmosphere that significantly affects the plasma stream. The origins of this patchy SO_2 atmosphere are the volcanoes and the subsequent sublimation of frost ejecta. Ionization caused by the impact of the neutrals with electrons from the plasma torus as well as photo-ionization (to a lesser extent) generate an ionosphere around Io. Additional ionization caused by field aligned electron beams (see Section 1.6.6) is thought to contribute to the dense wake of stagnant plasma observed downstream of Io (*Frank and Paterson*, 1999; *Hinson et al.*, 1998; *Saur et al.*, 2002; *Dols et al.*, 2008).

Focusing on the electromagnetic interaction, the relative motion of Io with respect to Jupiter's magnetic field causes a motional electric-field across Io. Electric currents can consequently flow from the Jovian side of Io to the anti-Jovian side, owing to the conductivity of Io's ionosphere. These currents force the incoming plasma to strongly slow down upstream of the moon. Only a small part of the torus particles can penetrate into the ionosphere while the remainder is directed around Io and accelerates around the flanks. The addition of newly created plasma into the flux tubes generates mass loading and slows the bulk flow, since these particles were initially at rest compared to Io. At the same time, the charge separation that immediately follows the ionization causes pick-up currents, since the electron gyro-center is shifted towards Jupiter while the ion gyro-center is shifted away from the planet. However, calculations from *Saur et al.* (2003) show the main contributor to the strong Io-plasma torus interaction is the elastic collisions between ions and atmospheric neutrals rather than the mass loading.

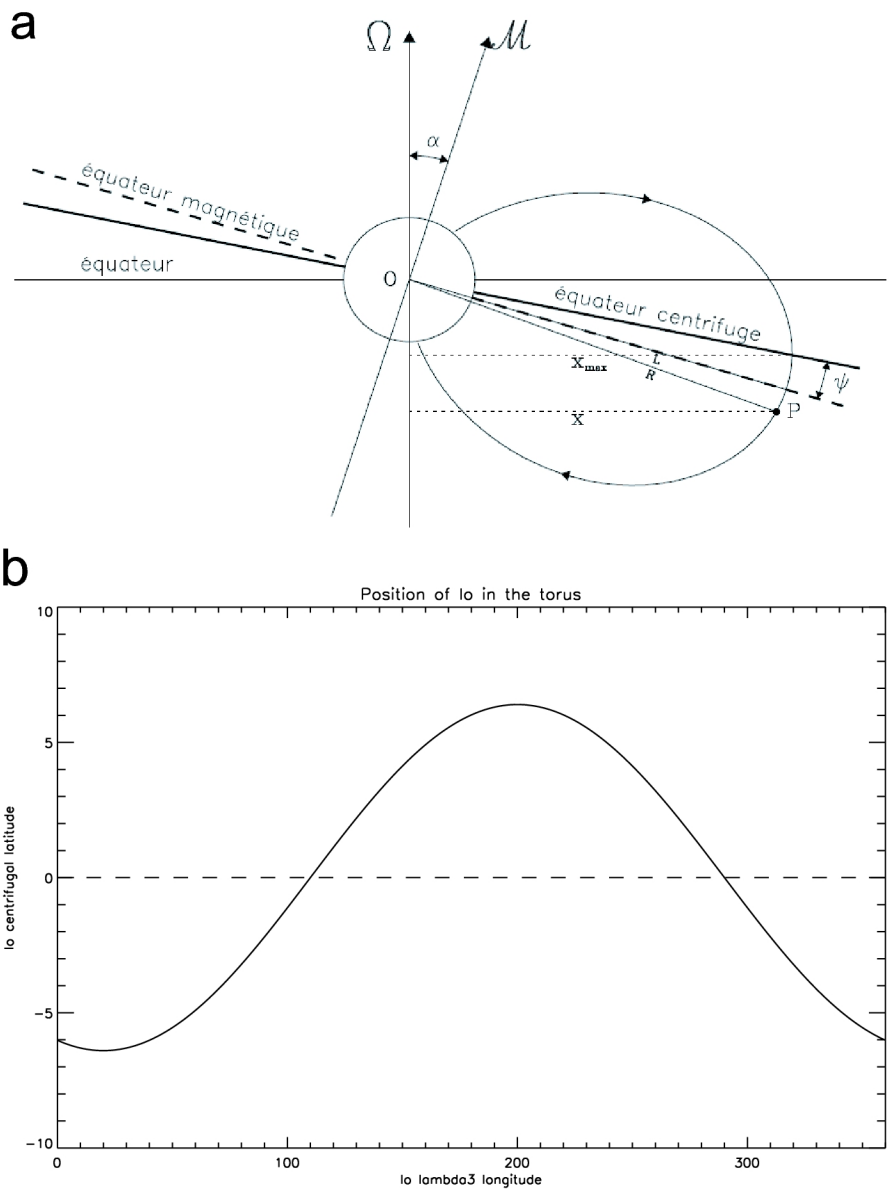

Figure 1.6: (a) Illustration of the torus centrifugal equator (thick solid line) compared to Io's orbital plane (thin solid line) and to the Jovian dipolar equator (dashed line). Ω represents the Jovian rotation axis and M represents the magnetic field dipolar axis. (From *Moncuquet* (1997)) (b) Plot of the centrifugal latitude of Io in the plasma torus as a function of its System III longitude.

1.5.4 The far-field electromagnetic interaction

1.5.4.1 The Alfvén waves

In ideal magneto-hydrodynamics (MHD) applied to compressible fluids, three wave propagation modes can be found. Two of them are compressional modes and thus imply density variation in the plasma. These waves are called the fast and the slow magneto-sonic waves. The last mode has an intermediate phase speed, is a transverse mode only and is called an Alfvén wave. Out of the three modes, only the Alfvén waves are able to carry an electric current. Nevertheless, the electric field does not vary along the magnetic field lines (i.e. in the parallel direction). Consequently, these waves are normally not able to accelerate electrons along the field lines. However, when the ideal MHD conditions are no longer fulfilled, dispersive effects arise, i.e. kinetic and inertial effects. When dispersive corrections are accounted for, a parallel component arises for the electric field and thus electron acceleration becomes possible. The corrections related to the electron inertia are expected to become important close to Jupiter, where the electron thermal speed is small compared to the Alfvén speed. On the other hand, the kinetic effects are expected to arise when the plasma becomes denser and the magnetic field weaker, which is the case closer to Io. However, *Jones and Su* (2008) argued that both effects compete within the plasma torus, leading to a weak electron acceleration at low centrifugal latitudes. Outside the torus, the inertial term clearly dominates and the related parallel electric field is maximum approximately $1R_j$ above the planetary surface. Finally, the authors suggest that this parallel electric field is directed planet-ward during a half phase and anti-planet-ward during the other half phase, leading to electron acceleration in both directions.

1.5.4.2 The unipolar inductor

The early models of the interaction between Io and Jupiter have been proposed by *Piddington and Drake* (1968) and *Goldreich and Lynden-Bell* (1969) to explain the Io-related radio emissions (see Section 1.6.5). The principle of the unipolar inductor is relatively simple. The motion of a conductive body embedded into a magnetic field induces an electric field perpendicular to the magnetic field and to the motion direction. In our case, since the magnetic field is oriented from North to South and since Io is rotating counter-clock wise (as viewed from the North), this motional electric field direction is anti-Jovian. The electric circuit is

closed through supposedly perfectly conducting magnetic field lines and through the Pedersen current in the Jovian ionosphere (see Figure 1.7). According to this model, the Io-Jupiter interaction is modeled as a direct current flow between the moon and its planet. The current flows from Io along one-half the surface of the Io flux tube (i.e. the field lines passing through Io) and flows in the other direction in the other half. Initially, the current was supposed to circulate through Io's interior, but this assumption was later replaced by Pedersen and Hall currents in Io's ionosphere. In this model, the conductivity of the satellite and of the field lines are assumed infinite, so that the intensity of the current is only limited by the Pedersen conductivity in Jupiter's ionosphere. *Goldreich and Lynden-Bell* (1969) computed that such current would reach $1.1 \times 10^6 A$. In this theoretical framework, the magnetic force on the current which flows through Io gives rise to a torque which transfers angular momentum from Jupiter's spin into Io's orbital motion[3]. The perturbed field lines are then bended in the downstream direction with respect to Io. These authors computed a lead angle[4] of 12°. In this model, the auroral footprint would thus lie at the foot of the perturbed flux tube.

It is noteworthy to state that the direct current model has always been considered by their authors as a simplifying hypothesis. The interaction was assumed to propagate in the form of Alfvén waves and the assumption was only valid if the perturbation reflected at the Jovian ionosphere was able to reach Io before the satellite moved away. However, this hypothesis seemed reasonable since the magnetosphere of Jupiter was considered as a very tenuous medium and the Alfvén speed was assumed close to the speed of light (see next section).

1.5.4.3 Alfvén wing model

After the Voyager encounters, the ability of the Alfvénic perturbation to come back to Io before the satellite moved significantly due to orbital motion was questioned

[3]This statement has been made assuming that Io's interior was the conducting body. Later evolutions postulated that momentum was instead transferred to the newly created Iogenic plasma.

[4]In this context, the lead angle is the longitudinal difference between the foot of an imaginary unperturbed field line passing through Io and the foot of the perturbed field line. We will see later that the lead angle is now often used to refer to the longitudinal difference between the foot of the unperturbed flux tube and the observed Io footprint. The discrepancy is that it is no longer assumed that the observable footprint lies at the foot of the perturbed flux tube.

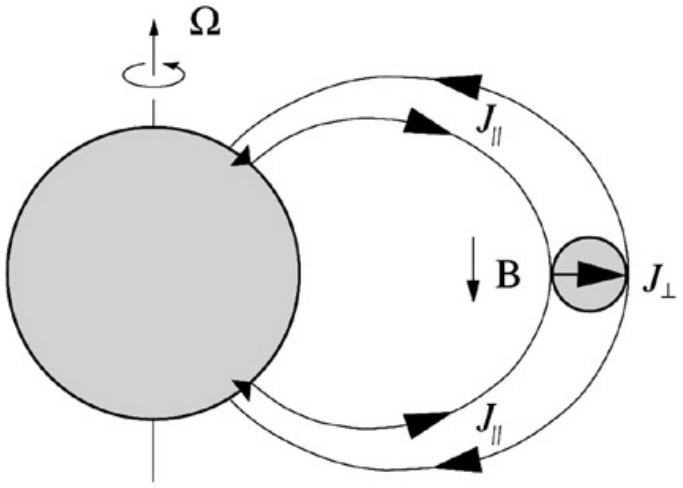

Figure 1.7: Schematic illustration of the unipolar inductor mechanism. The motion of Io in Jupiter's magnetosphere induces an electric field across the moon. Since the Iogenic ionosphere is conducting, a current can flow from the Jovian to the anti-Jovian side of Io and close through the magnetic field lines and Pedersen currents in Jupiter's ionosphere. (From *Thomas et al.*, 2004)

because the speed of the Alfvén waves strongly depends on the plasma density[5] and the spacecraft fly-bys had just unveiled the existence of the dense plasma torus. Other models were thus proposed to describe the propagation of the Alfvén waves without the direct current circuit hypothesis. In these models, the current does not flow along the magnetic field lines but is aligned with the characteristics of the Alfvén waves, called the Alfvén wings (*Neubauer*, 1980) (See Figure 1.8). In a simplified picture, the Alfvén waves propagate along the field lines and the field lines are drifting away from Io. Since the Alfvén speed is limited, especially in the dense torus, the perturbation propagates obliquely relatively from Io and the locus of perturbed points forms the Alfvén wings. The round trip Alfvén propagation time is estimated around ∼1200 seconds when Io is in the center of the torus (*Crary and Bagenal*, 1997). The maximum lead angle computed from Voyager derived torus density profiles is $\sim 8^\circ$ (*Prangé et al.*, 1996).

As discussed by *Neubauer* (1980) and confirmed both numerically and analytically by *Wright* (1987) and *Wright and Schwartz* (1989), the Alfvén waves experience

[5]
$$\mathbf{V}_{Alfven} = \frac{\mathbf{B}}{(\mu_0 \rho)^{1/2}}$$
where $\mathbf{V}_{Alfven}$ is the Alfvén speed, $\mathbf{B}$ is the magnetic field vector and ρ is the mass density.

reflections owing to density and magnetic field gradients both at the Jovian ionosphere and at the torus border. These reflections can lead to different interference patterns and thus generate multiple spots in the footprints or multiple radio arcs.

1.5.4.4 Electron acceleration mechanisms

The above model describes how the current flows between Io and Jupiter but does not really explain how this current accelerates the particles from a few eV in the torus to keV when precipitating into Jupiter's ionosphere. A first explanation could be that, when a field aligned current reaches a low density region at high latitude, the number of charge carriers decreases and the particles of this region are accelerated in accordance with the conservation of the current. On the other hand, another model suggests that the magnetic shear at high latitude could enhance parallel electric fields through resistive instabilities (*Kopp et al.*, 1998). A third model also proposed that the strong current flowing between Io and Jupiter could generate ion-cyclotron waves that could then excite kinetic Alfvén waves. These low frequency kinetic Alfvén waves could in their turn accelerate particles along the magnetic field lines (*Das and Ip*, 2000). Finally, *Crary* (1997) argued that Alfvén waves are totally reflected by the density gradients at the torus border so that no energy could reach Jupiter in this form. However, by considering the finite electron inertia, this author proposed that the electric field associated with the kinetic Alfvén waves could accelerate electrons inside the torus trough repeated Fermi acceleration. However, as described above, the most likely candidates to accelerate the precipitating electrons are the electric fields created at high latitudes when inertial effects in the Alfvén wave propagation become significant (*Jones and Su*, 2008).

1.5.4.5 Further evolutions of the models

Galileo in situ measurements showed that the field lines are strongly slowed down after contacting Io, leaving more time for the Alfvén waves to come back close to their emission points. As a consequence, models similar to the unipolar inductor were again seen as a possible solution. For example,*Crary and Bagenal* (1997) proposed a hybrid model in which the interaction begins as an Alfvénic disturbance and evolves downstream to a direct current loop. *Pontius* (2002) proposed a formulation of the wing current that combines properties of the unipolar inductor model with others from the Alfvén wing model. *Saur et al.* (2004) describe the unipolar induc-

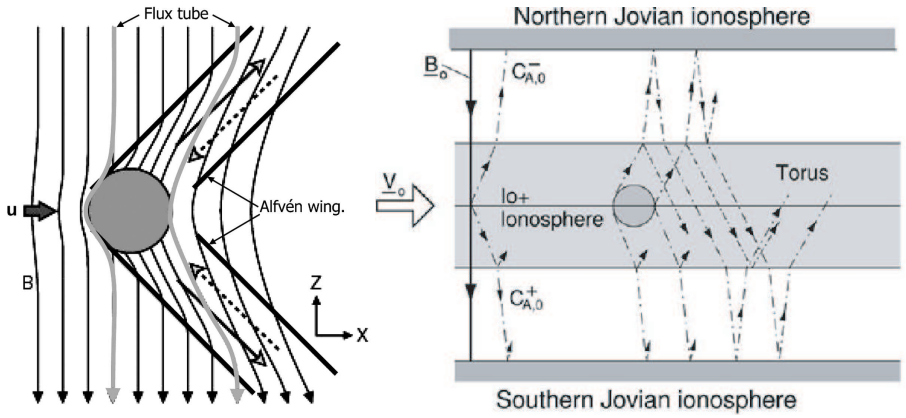

Figure 1.8: (Left) Side view illustration of the Alfvén wings model. The thin dark vertical lines represent the magnetic field lines while the Alfvén wings are represented with bold oblique lines. The Io flux tube is shown in grey. (From *Kivelson et al.*, 2004) (Right) Scheme of the possible reflections of the Alfvén wings. Reflections can occur at the inner boundary of the torus, in the Jovian ionosphere or at the outer boundary of the torus, leading to different reflection patterns. (From *Saur et al.*, 2004)

tor model and the ideal Alfvén wing model as two extreme cases of a more general description of the Alfvén waves propagation. The intermediate situation is called the mixed Alfvén wave disturbance system and it involves only partial feedback between Io and the reflecting boundary[6]. Recently, *Jacobsen et al.* (2007) used a 3D non-linear MHD simulation to study the propagation and the reflection of the Alfvén waves when the Io-plasma interaction is nearly saturated (i.e. when the plasma is nearly stopped relative to Io, in accordance with the observations). According to their simulations, the strength of the interaction strongly influences the propagation pattern. They notably found that, in case of strong interaction, the reflected waves can be nearly anti-parallel to the incident direction. They also showed that constructive and negative interferences take place, modifying the current pattern and thus influencing the auroral footprint morphology.

The plasma wave instrument on board Galileo also recorded intense electromagnetic waves at frequencies up to several times the proton gyro-frequency when crossing the Alfvén wings. *Chust et al.* (2005) interpreted these "high frequency/small scale" electromagnetic waves as the signature of the filamentation of the Alfvén

[6]In the ideal Alfvén wing model, no feedback does exist and the Alfvénic conductivity controls the electric current while in the unipolar inductor case, the feedback is strong and the Jovian ionospheric Pedersen conductivity controls the current.

waves. According to these authors, filamentation can transfer energy from large scale Alfvén waves into smaller scale waves which could transfer energy through the torus boundaries more efficiently.

1.5.4.6 The trailing trail

The discovery of an extended wake of plasma downstream of Io as well as the observations of a more than 100° long trailing tail emission downstream of the brightest spot gave rise to new models describing this feature of the footprint (*Hill and Vasyliūnas*, 2002; *Delamere et al.*, 2003; *Ergun et al.*, 2009). *Delamere et al.* (2003) divide the Io-plasma interaction into 3 phases. Phase I consists of the interaction between the corotating flux tube and Io, as described in the above sections. Phase II describes the acceleration of the wake plasma by an electrodynamic coupling with the surrounding torus plasma[7] before the Alfvén waves have reached the torus boundary. This coupling does not accelerate completely the wake plasma and the full corotation can only be achieved when coupling with Jupiter's ionosphere is attained. Phase III is the quasi-steady state weak coupling to Jupiter. During this last phase, these authors assume that high latitude field aligned electric fields are generated when the sub-corotating flux tubes decouple from Jupiter. These electric fields are thought to accelerate the electrons that cause the trailing tail auroral emissions. The other two models only focus on Phase III but they do not postulate such a decoupling between the flux tubes and the ionosphere. The model from *Hill and Vasyliūnas* (2002) is more similar to the unipolar inductor model. It is based on the assumption that the finite ionospheric Pedersen conductivity limits the current flowing between the wake plasma and Jupiter and thus prevents the charged particles to immediately reach full corotation. The *Ergun et al.* (2009) model is based on the same formulation, but they added a new current-voltage relationship which models a quasi-static potential drop to accelerate the tail electrons.

1.6 Observations

The Io-plasma torus interaction can be probed with a variety of observational tools. Each one provides a different contribution to the understanding of the physics of the phenomenon. Some have been acquired from ground based observatories, some

[7] I.e. the unperturbed corotating plasma.

required a space telescope and the last type consists of in-situ measurements or close images from interplanetary probes.

1.6.1 The Infrared footprint

The first detection of the auroral footprint of the Io-torus interaction was achieved at the $3.4\mu m$ infrared (IR) wavelength (*Connerney et al.*, 1993). These images were obtained with the 3-m telescope of the Infrared Telescope Facility (IRTF) at Mauna Kea, Hawaii. The observed IR emissions are dominated by the H_3^+ molecular ion. Ionization of the H_2 molecule by electron impact creates an H_2^+ molecular ion. This ion then quickly interacts with another H_2 molecule to form an H_3^+ molecular ion plus a hydrogen atom. Since H_3^+ is formed at the base of the thermosphere, its emissions are not affected by the absorbing layer located below the methane homopause. On the other hand, all emissions from lower altitudes, such as thermal emissions from Jupiter or reflected sunlight, are strongly weakened, so that the contrast between auroral emissions and background emissions is very pronounced.

Connerney et al. (1993) measured the longitudinal spacing between the location of the Io footprint and the foot of the unperturbed field lines passing through Io according to the O6 magnetic field model. This angle ranged from 15° to 20° and was systematically a lead angle, i.e. the location of the footprint is located downstream of the orbital position of the moon. They argued that these values are considerably larger than the angle expected from the Alfvén wings theory. Additionally, they found no correlation between the lead angle and the System III location of the footprint. Finally, they suggested that the non-detection of the northern footprint in the area where the magnetic field was the strongest could be an indication that the ionosphere Pedersen conductivity was playing a role in the footprint brightness. Consequently, the authors concluded that these elements were in favor of a strong unipolar inductor interaction controlled by the Pedersen conductivity of the ionosphere of Jupiter.

Connerney et al. (1998) used the location of the Io footprint on IRTF infrared and HST FUV images in order to constrain magnetic field models. Indeed, the location of the footprint provides information on the polar surface magnetic field that is not accessible with probes remaining in the equatorial plane. Consequently, the authors derived a 4th order spherical harmonic model constrained by in-situ measurements provided by the magnetometers onboard Voyager 1 and Pioneer 11

and by the mapping of the Io footprint positions into the equatorial plane. This model is called VIP4 for Voyager Io footprint Pioneer 4th order model.

IR images also suggested that some emission was sometimes present 10° downstream from the beginning of the spot. Additionally, *Connerney and Satoh* (2000) reported the presence of multiple spots separated by 5° downstream from Io. They noted that spot multiplicity is more in agreement with the Alfvén waves theory. A possible explanation for the presence of these previously unidentified features could be the improvements of the IRTF instrument and the image processing techniques and/or the increase of the torus density in the 1998-1999 era. However, the image shown in Figure 6 of *Connerney and Satoh* (2000) is peppered by speckles usually related to deconvolution algorithms, which sheds some doubts on the existence of this chain of spots.

In conclusion, the ideas concerning the Io footprint theoretical explanations evolved in response to the increase of the observational database and to the improvements of the instruments and data processing. The lead angle measurements were first in favor of the unipolar inductor but the discovery of secondary spots was then considered as a strong argument strengthening the Alfvén wings theory. We will see in the next section that the conclusions based on the analysis of the UV footprint followed a similar evolution.

1.6.2 The ultraviolet footprint

We have seen in the previous section that observation through near infrared windows is possible from ground observatories. Unfortunately, the far ultraviolet wavelength range is not accessible from Earth because of the strong absorption by the atmosphere. Accordingly, observations of the Jovian UV aurorae are only achieved from space telescopes. The most powerful one at this time is the 2.4 m wide Hubble Space Telescope (HST). All the studies of the Io UV footprint have been done with its successive cameras. Figure 1.9 illustrates the evolution of the Jovian aurorae FUV imaging performances with these different instruments. Unlike IR emissions, which are believed to be thermalized, either by precipitation induced collisional heating or by Joule heating, the FUV emissions result directly from collisional excitation of H_2 and H atmospheric particles with electrons. Jovian FUV auroral images include H_2 Lyman band emissions as well as the Werner band series, plus the H Lyman-α line. In this study, we both considered images including or rejecting H Lyman-α

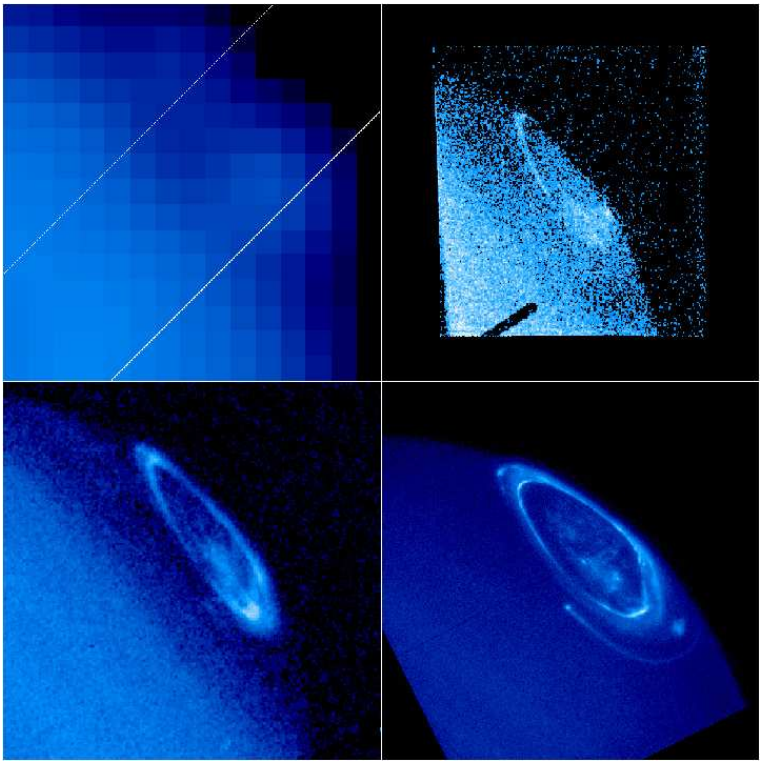

Figure 1.9: Comparison of UV images of Jupiter's aurora from IUE (simulated, upper left), HST post-COSTAR FOC (upper right, 716 sec), HST WFPC 2 (lower left, 500 sec), and HST STIS (lower right, 120 sec). Each of these images is of the northern aurora near 180° CML, and they are presented with the "pipeline" processing and background subtraction for an equal comparison. For the IUE panel, the WFPC 2 image has been convolved with a 6 arcsec FWHM function to simulate the IUE angular resolution within the large aperture (marked with white lines). (From *Clarke et al.*, 2004)

emission.

A controversy exists on the first discovery of the Io UV footprint. *Prangé et al.* (1996) claimed that they demonstrated the existence of the UV footprint on one image acquired with the Faint Object Camera (FOC) onboard the Hubble Space Telescope. On the other hand, *Clarke et al.* (1996) estimated that this single observation did not identify the Io footprint by itself and they brought stronger evidences of the presence of the Io UV footprint on Wide Field Planetary Camera 2 (WFPC2[8]) images. However *Prangé et al.* (1998) presented a new set of FOC images showing

[8]The WFPC2 camera is another imaging camera onboard HST that provides a better signal to noise ratio than FOC but a reduced angular resolution (0.0455 arcsec per pixel).

	Emitted power	Input power	Brightness
Prangé et al., 1996	5×10^{10}W	$2 - 3 \times 10^{11}$W	700 kR
Clarke et al., 1996		10^{11}W	60-120 kR
Prangé et al., 1998		$0.8 - 5 \times 10^{11}$W	
Clarke et al., 1998			35-250 kR
Gérard et al., 2006		$0.4 - 8 \times 10^{10}$W	25-220 kR
Sério and Clarke, 2008			40-480 kR

Table 1.1: List of the published emitted and electron precipitated power for the FUV Io footprint. For the *Gérard et al.* (2006) paper, the printed value is 0.4-8 GW but, after verification, it appears that this 10 times smaller value came from a typo in a conversion coefficient. We thus considered here the corrected value.

the Io footprint as well as its trailing tail.

Similarly to the Infrared wavelength observations, the measurements of the lead angles[9] were thought to be the best way to discriminate the unipolar inductor model from the Alfvén wings model. Lead angles between 0 and 15° were also found in UV but none of these results led to firm conclusions because of the expected inaccuracy of the magnetic field models. Moreover, lag angles (i.e. negative lead angles) have been reported (*Prangé et al.* (1998); *Clarke et al.* (1998); *Gérard et al.* (2006)), even though they do not make sense according to all current theories.

As far as the involved input power and emitted brightness are concerned, the published values range respectively from 4 to 300 GW and from 25 to 700 kilo-rayleighs[10] (kR). These numbers are compiled in Table 1.1.

The next generation UV camera was the Space Telescope Imaging Spectrograph (STIS). This instrument combines the resolving power of the FOC camera[11] with an unprecedented sensitivity. Several major breakthroughs have been made with this camera such as the discovery of secondary spots downstream of the main one (*Clarke et al.*, 2002). The proximity of these multiple spots first suggested that they all belong to the interaction region close to Io. Nevertheless, a more detailed study by *Gérard et al.* (2006) demonstrated a link between the inter-spot distance and

[9]The lead angle is defined here as longitudinal difference between the foot of undisturbed field lines passing through Io and the actual footprint location.

[10]1kR=10^9 photons cm^{-2} s^{-1} into 4π steradians

[11]The FOC angular resolution is 0.014 arcsec per pixel, but, practically, these images have to be re-binned to 0.028 arcsec per pixel in order to be usable. The situation is nearly identical with STIS since a high resolution (0.012 arcsec per pixel) mode does exist, but is generally not used because it does not bring any quality improvements. The STIS resolution is then fixed to 0.024 arcsec per pixel.

the location of Io in the torus (see Figure 1.10). When Io is close to the northern border of the torus, the northern footprint is faint and the inter-spot between the two first spots is maximum. The situation is the same for the southern footprint when Io is south. Alternatively, when Io is located in the center of the torus, its brightness is maximum and only a unique spot is visible in each hemisphere. The authors thus concluded that Alfvén waves reflections on the inner border of the plasma torus would qualitatively explain the evolution of the inter-spot distance. They also showed a similar correlation between the main spot brightness and Io's latitude in the torus (see Figure 1.11). This correlation had already been searched in WFPC2 data, but unsuccessfully because of the lack of data (*Clarke et al.*, 1998). The authors suggested that the plasma density controls the brightness since the IFP brightens when it approaches the dense torus center and vanishes when it approaches the borders. Based on a larger set of STIS data, *Serio and Clarke* (2008) confirmed the link between the brightness and Io's centrifugal latitude. They attributed this behavior to the increase of the collision rate and mass loading when Io approaches the dense torus center.

STIS observations from *Clarke et al.* (2002) also clearly confirmed the FOC observations (*Prangé et al.*, 1996) of the long trailing tail up to 100° behind the footprint. The authors argued that this tail could not be due to some afterglow but is linked to high energy particle precipitation.

Another controversial topic is the spatial extent of the Io footprint. FOC images seemed to indicate that the size of the footprint was comparable to the projected size of Io in the ionosphere (*Prangé et al.*, 1996; *Prangé et al.*, 1998). Consequently, these observations suggested that the interaction region in the equatorial plane was confined within a few Io radii. Nevertheless, the estimated size was based on the measurement of the footprint latitudinal width and not on the longitudinal length. As far as the length is concerned, the elongation measured up to 4.5° and was attributed to the blurring owing to long exposure times (from 535 to 1421 seconds) combined with the distortion of the magnetic field lines. On the other hand, WFPC2 observations lead to footprint as long as 1000-2000 km even after correction of the rotational blurring(*Clarke et al.*, 1996) while STIS observations gave lengths between 500 and 3000 km (*Clarke et al.*, 2002). These measurements thus suggested that the interaction region was more than 10 times larger than Io. Nevertheless, in the *Clarke et al.* (2002) paper describing the STIS results, the authors assimilated both primary and secondary spots to the interaction region. In their interpretation of the footprint

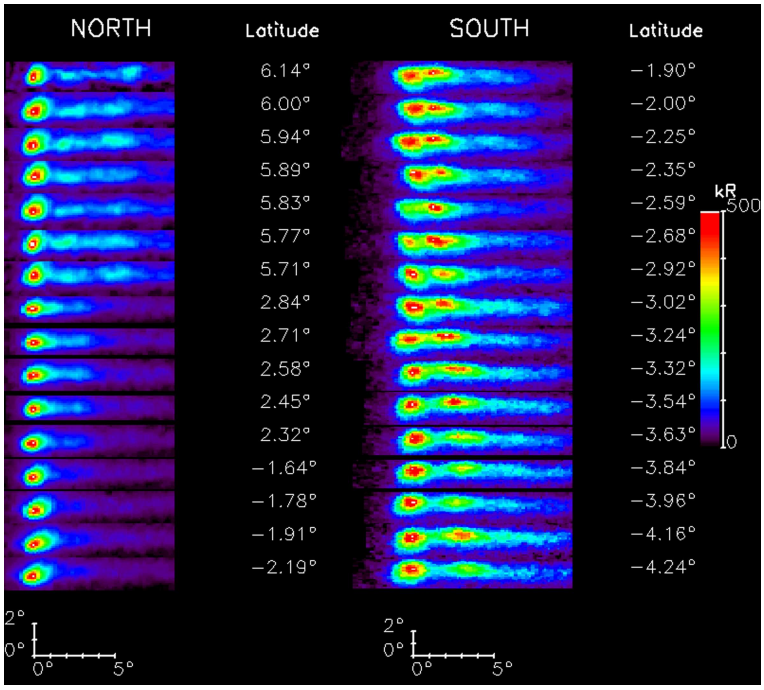

Figure 1.10: Samples of rectified traces of the Io footprint as a function of the centrifugal latitude of Io. It is noticeable that multiple spots are observed in the northern hemisphere when Io is close to the northern torus boundary (and vice-versa for the southern footprint). On the other hand, only one spot can be identified when Io is close to the torus center. (From *Gérard et al.*, 2006)

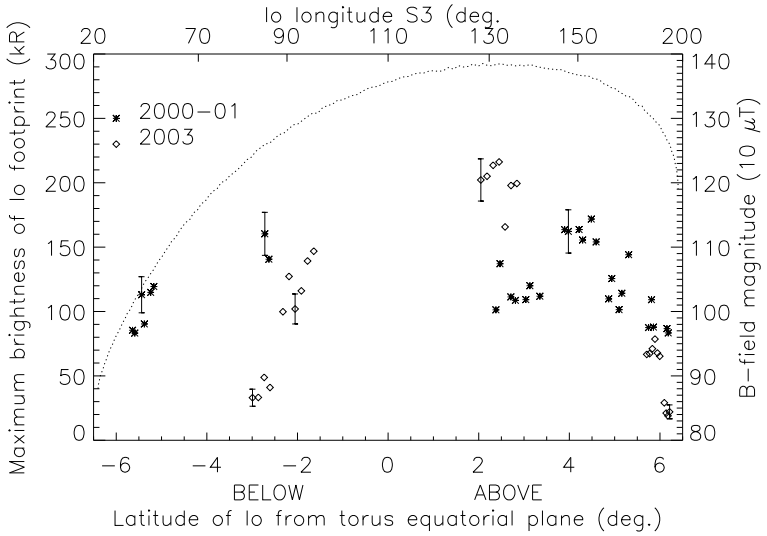

Figure 1.11: Plot of the maximum brightness of the northern main spot as a function of the centrifugal latitude of Io in the torus. The dotted line represent the surface magnetic field magnitude of the foot of the Io flux tube. We can see that the main spot is brighter when is is close to the dense torus center while its brightness decreases when Io is close to the torus border. (From *Gérard et al.*, 2006)

morphology, *Gérard et al.* (2006) separated the different spots. By measuring the size of the first spot only, they came to the conclusion that the size of the spot ($\sim 0.9°$) approximately corresponds to the size of Io when mapped back into the equatorial plane along the field lines. Finally, *Serio and Clarke* (2008) reported estimates of the IFP diameter as measured perpendicularly to the downstream direction. Their values range from $\sim$ 500 km to $\sim$ 2000 km.

Early estimates of the IFP color ratio led to the conclusion that the energy of the precipitating electrons was similar to the energies related to the main oval (*Clarke et al.*, 1996). Later and more detailed studies with the GHRS and the STIS spectrographs led to the conclusion that the IFP electrons have a mean energy definitively less than electrons precipitated into the main auroral oval, typically on the order of 55 keV[12] (*Dols et al.*, 2000; *Gérard et al.*, 2002). They also showed that the brightness drop in the tail was mainly caused by a drop of the electron flux rather than to a decrease of their mean energy.

[12]In comparison, the main oval precipitating electrons have an energy between 30 and 200 keV(*Gustin et al.*, 2004b).

1.6.3 The visible footprint

Additionally to the infrared and ultraviolet emissions, the Jovian aurorae also consist of visible emissions. The visible aurora is too weak to be detected against the bright reflected sunlight. However, the Galileo orbiter provided the first images of the aurorae at visible wavelength while orienting its camera on the night side. These unique observations provided by the Solid State Imager (SSI) instrument have been reported by *Ingersoll et al.* (1998) and by *Vasavada et al.* (1999).

The Io footprint is detected on 10 out of 24 images of the northern aurora acquired by Galileo from November 1996 to November 1997. The SSI clear filter (effective wavelength: 385-935 nm) is used for all these images and the exposure times are between 1.06 and 12.8 seconds. The System III Io longitudes range from 80° to 235° and the images come from 3 different Galileo orbits (C3, C10 and E11). Additionally to their unique wavelength, these observations provide an unprecedented spatial resolution between 26 and 134 km.

Vasavada et al. (1999) described the footprint as a circular patch with a FWHM diameter around 450 ± 100 km when Io has a System III longitude between 82° and 110°. On the other hand, *Ingersoll et al.* (1998) reported a more elongated spot with a FWHM size of 300×500 km and a full width (FW) of 500×1200 km. In a few images, the footprint appears as a pair of spots separated by 0.5° in longitude. In order to complete this morphological description, the SSI camera also detected a faint trailing tail similar to those observed in the UV and IR wavelength.

The observed lead angles range from 0° to 2° and the authors indicate that these numbers are more consistent with the Alfvén wings models than with the lead angle expected from the unipolar inductor. Finally, the maximum brightness is between 0.2 and 1 MR and the total power is estimated between 0.2 and 0.7 GW.

More recently, the LOng-Range Reconnaissance Imager (LORRI) visible panchromatic camera on board the New Horizons spacecraft also acquired visible images of the Io footprint (*Gladstone et al.*, 2007). On these images, the main spot width is around 400 km and its vertical extent is as large as 1000 km. Additionally, other spots are seen both upstream and downstream of the main ones (Figure 3.7).

1.6.4 Aurorae at Io

Usually, aurorae are found close to the poles, but on Io, auroral emissions are mainly located at the Jovian and anti-Jovian equatorial sides (Figure 1.12). According to

the model proposed by *Saur et al.* (1999), the divergence of the flow around Io caused by the electrodynamic interaction forces the electron flux tubes to reach preferentially the flanks of the satellite (*Saur et al.*, 2000). These auroral emissions are produced by impact excitation of neutral oxygen and sulfur atoms by hot electrons. Io's aurorae have been observed with HST, Galileo's Solid State Imager (SSI) and with ground-based observations (see review in *Saur et al.*, 2004). The spots rock up and down relative to Io so that they are located at the magnetic field tangent points (*Roesler et al.*, 1999). In FUV observations, the anti-Jupiter side is brighter, probably owing to Hall effect that rotates the electron flow and causes the hot torus electrons to enter Io's atmosphere preferentially by the anti-Jovian side (*Saur et al.*, 2000). However, on SSI images, the Jovian side frequently appears brighter. This opposite behavior has tentatively been attributed to a local concentration of molecular SO_2 from venting volcanoes (*Geissler et al.*, 2001). *Retherford et al.* (2007), based on FUV ACS images of Io during eclipses, confirmed that the location of the emissions is partly influenced by the location of the volcanic plumes. These authors also studied the relative influence of volcanoes and frost sublimation as sources of Io's atmosphere. They concluded, combining Io auroral images from ACS and from the Alice UV spectrometer on board New-Horizons, that volcanoes only provide 1 to 3% of the dayside atmosphere. FUV STIS observations showed that the equatorial spots brightness increases when Io is closer to the denser torus center (*Retherford et al.*, 2000). Similar results have been shown from ground-based [O I] 6300 Åmeasurements (*Oliversen et al.*, 2001). Short timescales (∼15-20 minutes[13]) and strong (typically ∼20-50 %) brightness fluctuations have also been observed and ascribed to fluctuations of the electron energy flux.

Additionally to the equatorial spots, faint polar glows have been observed both on visible (*Geissler et al.*, 2001) and FUV images (*Retherford et al.*, 2003) and appeared brighter on the pole closest to the centrifugal equator. These results suggested that this glow was generated by the interaction between Io's atmosphere and plasma torus electrons. Finally, enhanced emissions in Io's wake have been observed on STIS spectra by *Wolven et al.* (2001).

1.6.5 Io related radio emissions

Bigg (1964) has been the first to link some decametric radio emissions originating

[13]The detection of the exact timescale is limited by the sampling rate and thus could be smaller.

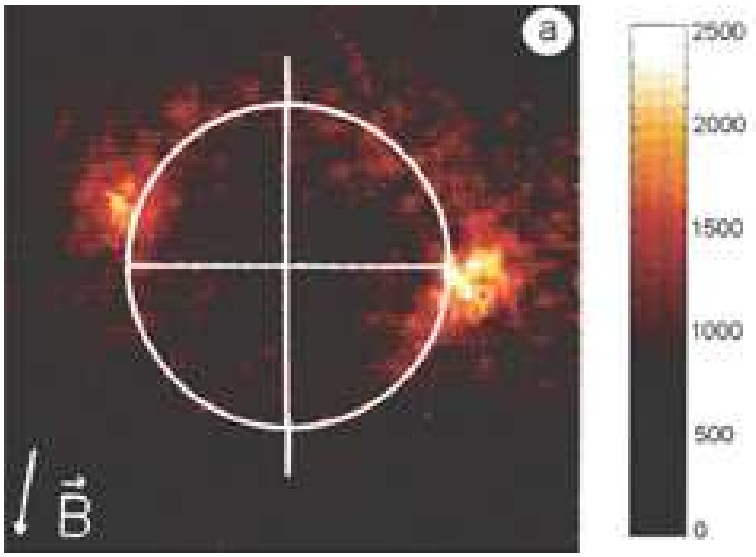

Figure 1.12: Image of OI 1356 Å Io's aurora. We can notice that the the spots are located at the tangent points relatively to the magnetic field lines. Additionally, the anti-Jovian spot is brighter (From *Roesler et al.*, 1999).

from Jupiter to the orbital position of Io. These Io related emissions are called Io-DAM (*Queinnec and Zarka*, 1998; *Saur et al.*, 2004). They occur when Io's phase angle is either close to 90° or close to 230°. Their frequencies range from ∼1 to 40 MHz and presumably correspond to the local electron gyro-frequency. According to the current magnetic field models, the lower frequency limit corresponds to an altitude of 1-2 R_J while the upper limit corresponds to the surface of Jupiter. The Io-DAM are elliptically polarized, but those which are dominantly right-handed originate from the northern hemisphere while the left-handed emissions are related to the southern one. These emissions appear as arcs in the frequency-time plane (i.e. in dynamic spectra) on timescales of minutes to hours. Four types of arcs are observed, noted A, B, C and D. A and B arcs are mostly right-handed while C and D are mostly left-handed. B and D arcs appear when Io is near dawn while A and D arcs occur when Io is near dusk. Each type has a specific shape in dynamic spectra. Figure 1.13 illustrates their different morphologies as they appear in dynamic spectra. The most widespread explanation for these arcs is that the radio waves are emitted along a conical sheet less than 2° thick and with a 70 ± 5° aperture half angle with respect to the magnetic field orientation. According to the magnetic field models, these arcs probably originate from field lines leading the unperturbed IFT by ∼10 to 30°. The orbital position of Io is not the only condition for Io-DAM occurrence. The arcs

are only observed when Io is in some specific locations in the magnetic field, with System III longitudes ranging from ∼170° to ∼310°, depending on the type of arc. These constraints appear as occurrence regions once translated into the CML-Io phase plane. Intense sporadic bursts on timescales of milliseconds, called S-bursts, are also observed a few percent of the time. They mainly consist in negatively drifting[14] features (see Figure 1.13d) and are consequently assumed to be associated with reflected electrons travelling from Jupiter to Io. Analysis of these S-bursts suggest electric potential jumps of ∼1keV accelerating electrons toward Jupiter and mostly localized at an altitude of 0.1 R_J, while the mean energy of the emitting electrons lies around 4 keV (*Hess et al.*, 2007). Moreover, *Hess et al.* (2009) showed that these acceleration structures can last for ∼10 minutes and move away from the planet. Additionally, new structures seem to appear every ∼200 seconds.

The Io-DAM generation mechanism is most probably the cyclotron-maser instability (CMI) and is related to unstable populations of electrons with energies from 1 to 10 keV. A necessary condition to the wave growth is that the gradient of the electron distribution function along the perpendicular velocity[15] axis is positive (see details in *Wu*, 1985). For example, this condition is encountered with loss cone distributions, in which a part of the electron population is lost into the atmosphere. This is the reason why the radio arcs are supposed to be directly related to the precipitating electrons leading to the footprint. Unfortunately, attempts to link radio and optical morphologies have been unsuccessful so far.

1.6.6 Electron beams at Io

The Galileo probe flew-by Io on six occasions and the Energetic Particles Detector (EPD) operated during 5 of these encounters (*Williams et al.*, 1996; *Williams et al.*, 1999; *Mauk et al.*, 2001; *Williams and Thorne*, 2003). Two of them occurred above the polar caps, one occurred in the wake region, one on the anti-Jupiter flank and one obliquely in front of the satellite (see Figure 1.14). Bi-directional electron beams have been identified on three (and possibly four) occasions out of these five cases. The half width of the beams is around 7°. The source altitude was estimated from these observations to be located around 0.6-0.7 Jovian radii (R_j) above the surface of Jupiter (*Williams et al.*, 1999). The PLasma Spectrometer (PLS) onboard Galileo

[14]By negatively drifting, it is meant that the frequency decreases with time.

[15]The velocity of a particle embedded into a magnetic field is usually decomposed into two components, one parallel to the field lines and one perpendicular to the field lines.

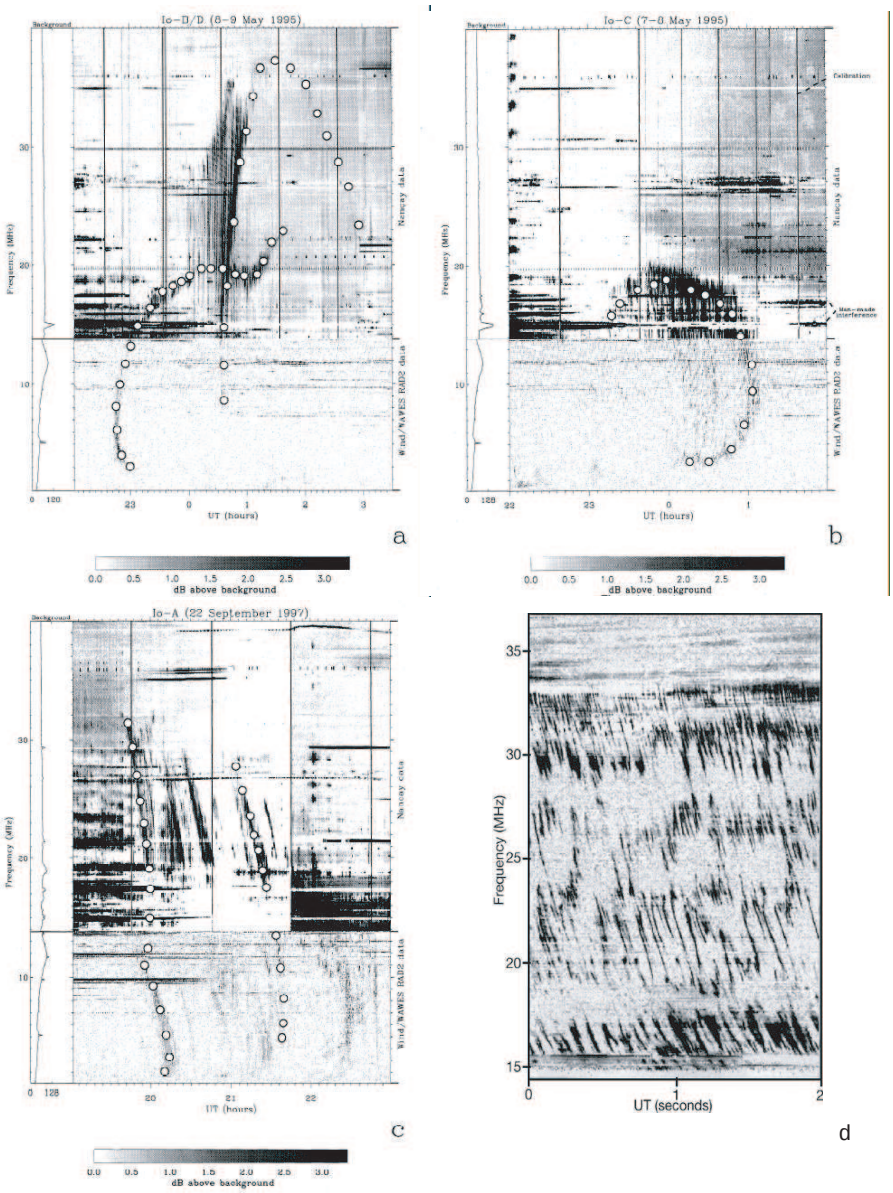

Figure 1.13: Examples of dynamic spectra of radio arcs. (a) B and D arcs. (b) C arc. (c) A arc. (d) Example of S-bursts. ((a), (b) and (c) from *Queinnec and Zarka*, 1998 and (d) from *Saur et al.*, 2004)

showed that the energy of these electrons extended towards lower energies (100 eV-1 keV) (*Frank and Paterson*, 1999; *Frank and Paterson*, 2000b; *Frank and Paterson*, 2002). After the first fly-by in the wake, these electron beams have been tentatively related to the UV footprints. *Frank and Paterson* (1999), for example, suggested that the beams could lead to a 3×10^{10} W total precipitated energy flux if the interaction cross section in the equatorial plane was 5400 km wide. Later fly-bys upstream and along Io's flank showed that the electron beams cross section was not extended in front and beside the moon. Since the electron beams cross section is much more restricted than previously proposed, the precipitated power deduced from UV footprint measurements appears hard to reach. Consequently, *Mauk et al.* (2001) proposed, by analogy with Earth processes, that these beams could originate from the planet-ward side of the current created by the Io interaction. Indeed on Earth, equatorward currents are associated with the electrostatic acceleration of electrons down into the atmosphere. On the other hand, FAST spacecraft in situ measurements also showed that the Earth-ward currents accelerate electrons towards the magnetosphere and thus create electron beams. The last encounters were polar fly-bys and revealed uni-directional Io-ward beams when flying over the Io polar caps, confirming the Jovian origin of source region (*Williams and Thorne*, 2003).

1.6.7 Galileo radio-occultation, magnetometer and plasma measurements

The finding of the electron beams were not the only valuable information obtained during these Io flybys. They also provided us with evidence of strong magnetic field perturbations taking place in Io's vicinity. Diversion and acceleration of the plasma flow have been observed around Io's flanks while stagnant plasma accompanied with a significant field depression were found in the wake region. Two scenarii were initially compatible with these measurements: the perturbations could have been attributed either to an internal magnetic field or to currents associated with the interaction between the plasma flow and Io's ionosphere or mass loading region. However, magnetic field measurements acquired during the two polar flybys finally led to the conclusion that Io has no appreciable internal field and that the observations can be fully explained with an Alfvénic model (see reviews by *Saur et al.*, 2004 and by *Jia et al.*, 2009a). Finally, radio occultation measurements reported by *Hinson et al.* (1998) indicate that the wake plasma is relatively quickly re-accelerated

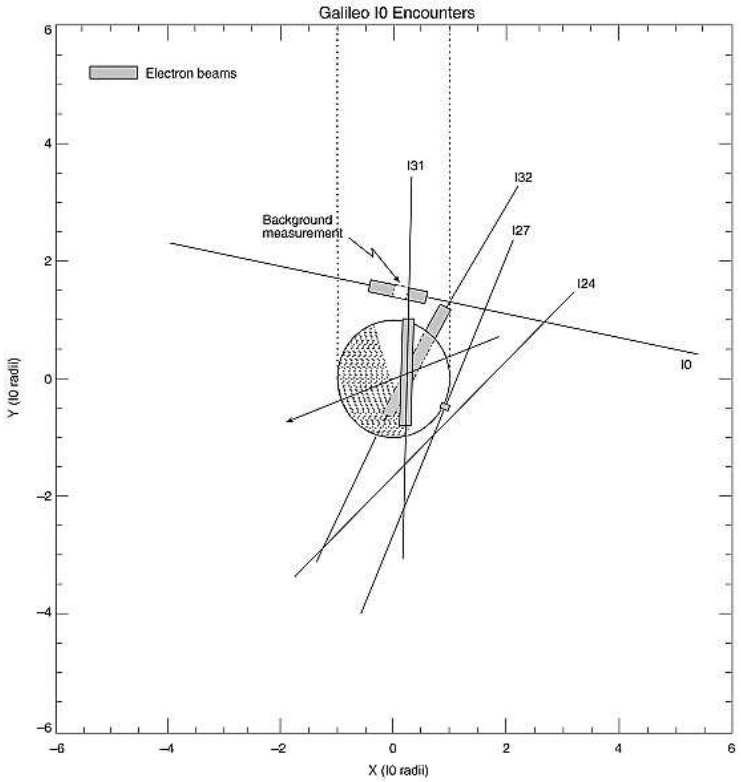

Figure 1.14: Location of the electrons beams as observed by Galileo EPD instrument. (From *Williams and Thorne*, 2003)

since it already reaches full corotation after 7 Io radii.

1.7 Description of the instruments

The present study is based on observations acquired with two UV cameras onboard the Hubble Space Telescope: the Space Telescope Imaging Spectrograph (STIS) and the Advanced Camera for Surveys (ACS). The UV channels of both instruments are based on the same technology: the Multi-Anode Microchannel Array (MAMA). Indeed, the detector of the ACS instrument is a flight spare model of the STIS detector. Figure 1.15 illustrates the design of these two detectors. The most important part of the device is the curved microchannel plate (MCP). Its upper face is covered by an opaque CsI photocathode. The MAMA is a photon counting detector. When a UV photon hits this layer, it produces a primary photoelectron that enters the microchannel. The electron cascade that follows produces a pulse of 4×10^5 secondary electrons at the exit of the MCP. The anode array then records the pulse and the signal is processed by the instrument electronics. The planar MgF_2 window above the device cuts off the wavelength shorter than 1150 Å. The field electrode between the MgF_2 window and the MCP is used to repel electrons that would be emitted away from the MCP back into the channel. The following sections describe these instruments with more details.

1.7.1 The Space Telescope Imaging Spectrograph

STIS is an imaging spectrograph that operates from near infrared to far ultraviolet (FUV) wavelength. The Space Shuttle crew installed it in February 1997 during the second servicing mission, together with the Near Infrared Camera and Multi-Object Spectrometer (NICMOS). The power system failed in August 2004, but the instrument was repaired during the last Space Shuttle servicing mission in May 2009. The prime capabilities of STIS are the spatially resolved spectroscopy from the UV to the near-IR (1150-10300 Å) and the echelle spectroscopy in UV. This versatile instrument also provides objective-prism spectroscopy and coronographic imaging. However, in this work, we are only interested in its imaging capabilities. STIS contains 3 different detectors:

- a CCD covering a 52×52 arcsec^2 field of view (FOV) and operating from 2000 to 10300 Å,

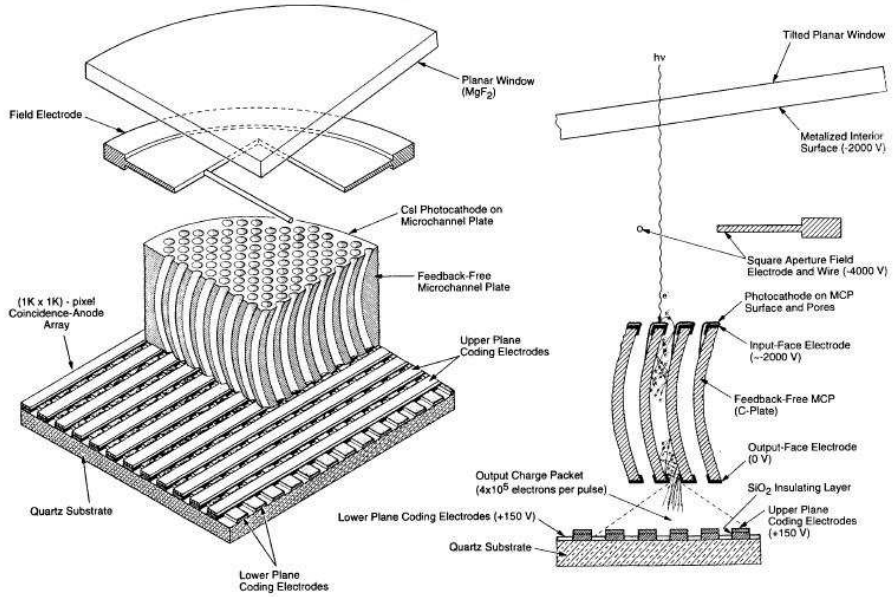

Figure 1.15: Design of the CsI MAMA detectors. This design is identical for STIS FUV-MAMA and the ACS SBC detectors. See the text for a more complete description. (From *Quijano et al.*, 2007))

- a Cs_2Te MAMA (NUV-MAMA) with a 25×25 arcsec^2 FOV and operating from 1600 to 3100 Å,
- a CsI MAMA (FUV-MAMA) covering a 25×25 arcsec^2 FOV and operating from 1150 to 1700 Å.

Since we are interested in the far UV H_2 Lyman and Werner as well as H Ly-α auroral emissions, only FUV-MAMA images have been used in this study. The two MAMAs have the unique capability of very high time-resolution (125 μs) imaging and spectroscopy. Two observation modes thus exist for STIS FUV-MAMA observations: the standard ACCUM mode, which produces images where the number of counts is accumulated for each pixel, and the TIME-TAG mode, which produces a list of detection events by recording the location and the arrival time of each count. Two filters have been mainly used: the CLEAR filter which includes the 1216 Å Ly-α band and the F25SRF2 filter (also known as the Strontium Fluoride filter) which mostly rejects this band. Figure 1.16 provides the throughputs of these filters as well as ACS's ones. Figure 1.17 compares the point spread functions of the STIS and ACS instruments for the four filters under consideration in this work. The full

widths at half maximum (FWHM) of these PSFs all lie between one and two pixels.

1.7.2 The Advanced Camera for Surveys

ACS has been installed in March 2001 in replacement of the Faint Object Camera (FOC) during servicing mission 3B. As its name suggests, this instrument is mainly designed for deep wide-field survey imaging of the sky (*Pavlovsky et al.*, 2006). Its main detector is a $2 \times 2048 \times 4096$ pixels CCD covering a 202×202 arcsec^2 field of view and operating in the visible and near-UV wavelength. Along with this Wide Field Channel (WFC) ACS has also two other high resolution channels. The High Resolution Channel detector is a CCD covering a 29×26 arcsec^2 field of view operating from 1700 Å to 11000 Å. The third channel, the one we are interested in, is the Solar Blind Channel (SBC). Its field of view is 35×31 arcsec^2 wide and its MAMA detector operates in the 1150-1700 Å range. The detector spatial resolution is 0.034×0.030 arcsec per pixel. The ACCUM mode is the only observation mode available. The HRC and the SBC share the same optical channel with the same corrective optics to compensate for the spherical aberration of the HST primary mirror. Prism spectroscopy is also available for the SBC channel but only its imaging capabilities have been used for this study. Like the STIS FUV-MAMA, the SBC MAMA has both local ($\geq$ 50 count/second/pixel) and global ($>$ 200000 count/second) maximum illumination rates. Because of its higher throughput, the total count rate is more limiting than for STIS and it constrains the observations to only the small portion of the planet including the polar regions while a larger part of the disk could fit into the field of view. Like for STIS images, two filters have been mainly used: the F115LP filter which includes H Ly-α band and the F125LP filter which rejects it.

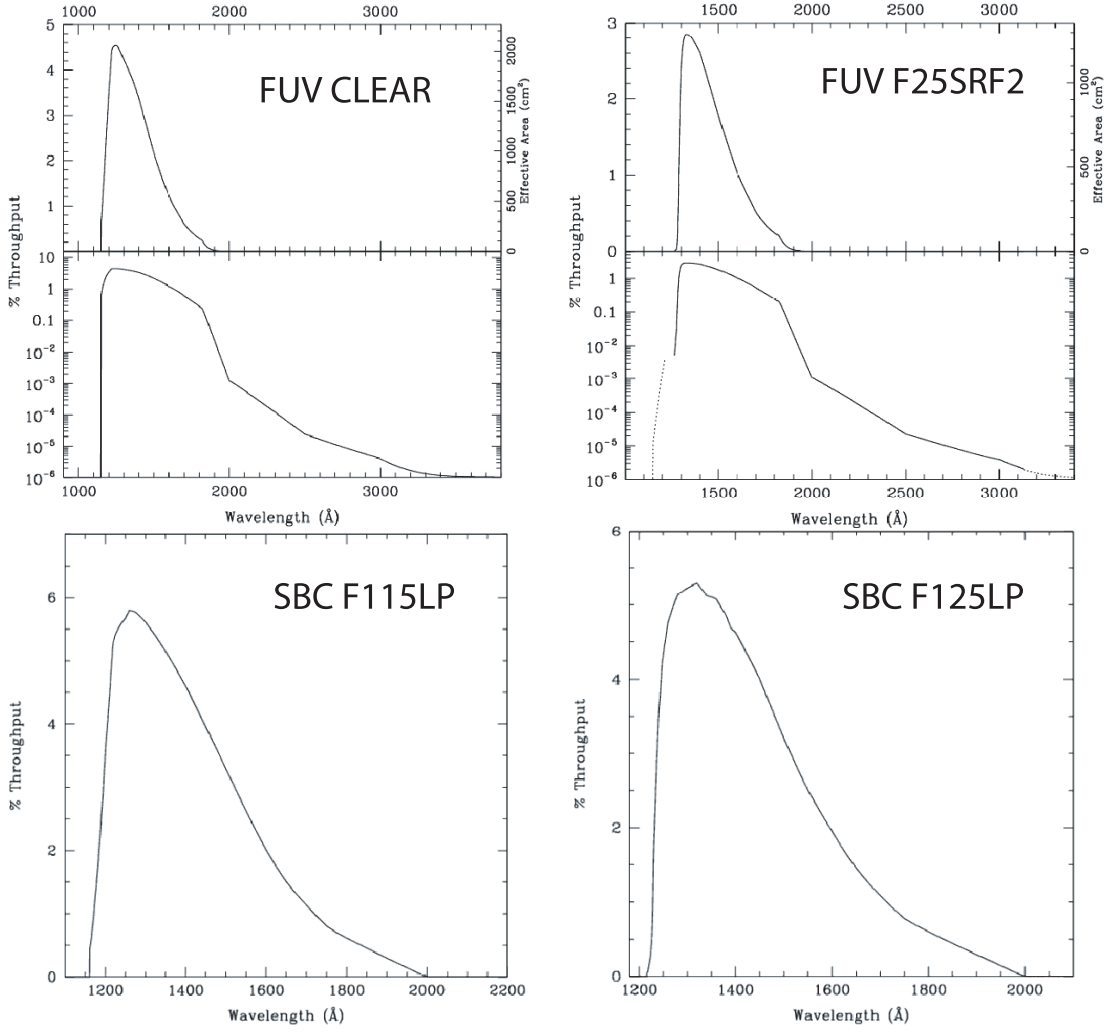

Figure 1.16: The two upper plots show the throughputs of the STIS CLEAR and F25SRF2 filters. The two lower plots show the throughputs of the ACS F115LP and F125LP filters. The CLEAR and F115LP filters have more or less the same characteristics but the ACS F125LP filter has a maximum throughput larger than 5% while the maximum throughput of the equivalent STIS F25SRF2 filter is less than 3%. (from *Pavlovsky et al.*, 2006)

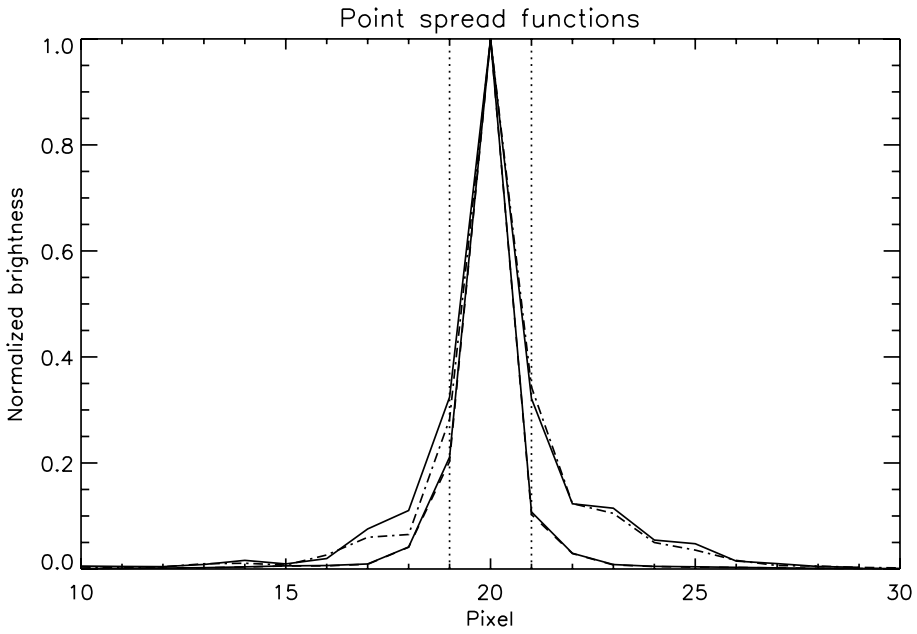

Figure 1.17: Comparison of the point spread functions for the four filters considered in this work. The solid line is for the F115LP ACS filter, the dashed line is for the F125LP ACS filter, the dash-dotted line is for the Strontium Fluoride STIS filter and the dash-dot-dotted line is for the STIS Clear filter. These PSF are computed with the TinyTim software (*http://www.stsci.edu/software/tinytim/tinytim.html*).